Yb–YAG laser offset welding of AA5754 and T40 butt joint

Giuseppe Casalino [a,*], Michelangelo Mortello [a], Patrice Peyre [b]

[a] DMMM, Politecnico di Bari, Viale Japigia 182, 70126 Bari, Italy
[b] PIMM, UMR 8006 CNRS, Arts et Métiers ParisTech, 151 Bd de l'Hôpital, 75013 Paris, France

A B S T R A C T

In this work, a 5754 Al alloy and T40 were joined in butt configuration by focusing a fiber laser onto the titanium side, close to the weld centerline (offset). The keyhole was made entirely of titanium, and the fusion of the aluminum was achieved by heat conduction. Neither filler metal nor chamfering was necessary to produce a sound, dissimilar weld. The assembly was free from porosity and spatter defects. The mechanical properties were satisfactory. The energy input, the laser offset, and their interaction had statistically significant effects on the ultimate tensile strength. The findings of this investigation prove the robustness and suitability of fiber laser offset welding for Al–Ti weld fabrication.

Keywords:
Yb–YAG laser welding
Al–Ti weld
Laser offset

1. Introduction

Joining processes of titanium with various materials are difficult to perform by conventional techniques, because of both the presence of a tenacious oxide coating on its surface and the limited titanium solubility in other metals. Mechanical processes such as riveting, clinching, and screwing are currently the most widely used joining techniques because they are not dependent on a metallurgical compatibility. Kreimeyer et al. (2005) obtained a structural phase transition during solidification and cooling of the weld. Peyre et al. (2014) proved that the formation of intermetallic compounds affects the quality of the assembly. Poor chemical affinity and metallurgical compatibility between the two metals can result in a non-homogeneous and brittle interface. Bondar et al. (2011) and Tomashchuk et al. (2015) conducted chemical and mechanical analyses on several intermetallic Al–Ti compounds to check their strength and ductility.

Several authors have proposed solid state welding. Luo and Acoff (2000) conducted an investigation of diffusion welding of Ti and Al multi-laminated materials. They showed that $TiAl_3$ intermetallic compounds form quite rapidly in the temperature range of 660–680 °C. During a study on friction stir welding (FSW) of Al–Ti, Dressler et al. (2009) shifted the tool pin center towards the Al plate. During the stirring action, the particles of Ti in the Al matrix elongated less than the surrounding Al, leading to the formation of cavities in the nugget zone. Chen et al. (2011a,b) pointed out the difficulties when performing FSW dissimilar butt welds because of their tendency to crack and to form grooves, especially due to the high rotation rate of the tool.

Other research showed good results related to laser fusion brazing welding. With this method, the laser light irradiates the aluminum that melts and wets the solid Ti surface. Alfieri et al. (2013) performed a preliminary investigation and presented a metallurgical characterization of the weld. Chen et al. (2010) found that an insufficient interfacial reaction layer morphology favors the initiation of cracks and reduces the mechanical properties of the joints. Song et al. (2013) demonstrated that the laser offset influences the thickness of the interfacial layer and can improve the mechanical properties of the weld but interfacial non-homogeneity, weld porosity and spatter defects reduce the joint quality. Chen et al. (2011a,b) showed that groove preparation and a uniform energy distribution prevent a non-homogeneous interfacial chemical reaction. Pastor et al. (1999) demonstrated the loss of magnesium, porosity and cracking during laser welding of the 5754 Al alloy. Therefore, focalization of the laser beam on the Al side often resulted challenging and negatively affected the seam quality.

To overcome the above-mentioned limitations, other authors have recently proposed the use of the fiber laser. Lee et al. (2013) investigated high-speed full penetration fiber laser welding of Ti and Al lap joints. The fiber laser can reduce the formation of intermetallic compounds. Ming et al. (2014) proposed fiber laser-cold metal transfer arc hybrid welding to join the Ti6Al4V Ti alloy and AA6061 Al alloy in butt configuration. They identified the setting of

* Corresponding author. Tel.: +0039 080 5962753; fax: +0039 080 5962788.
E-mail address: g.casalino@poliba.it (G. Casalino).

Table 1
Chemical composition of the as-received materials (% weight).

	Ti	Al	H	Mg	Fe	Mn	Si	Cr	O	Cu	N	C
T40	Balance	–	<0.02	–	<0.03	–	–	–	<0.25	–	<0.03	<0.10
5754 Al	<0.15	Balance	–	2.60–3.60	0.40	0.50	0.40	0.30	–	0.10	–	–

Table 2
Mechanical properties of the as-received materials: ultimate tensile strength (UTS), yield stress (YS), Young module (E), elongation to fracture (A%), Vickers microhardness (HV).

	UTS (MPa)	YS (MPa)	E (GPa)	A%	HV
T40	460	276	105	20	145
5754 Al	230	80	68	17	62

Table 3
Materials thermo-physical properties: thermal conductivity (K), fusion temperature (T_f), density (ρ).

	K (W/(m K))	T_f (°C)	ρ (g/cm^3)
T40	17	1930	4.51
5754 Al	147	870	2.66

process parameters that maximized the mechanical properties of the welds.

The aim of this paper is to study fiber laser offset welding (FLOW) of the 5754 Al alloy and T40 in butt configuration. The approach consisted in focusing an Yb–YAG laser onto the Ti side at a very short distance from the weld centerline, which was called offset. Unlike Möller et al. (2011), no filler material was used. Although Möller et al. (2011) and Vaidya et al. (2010) adopted filler wire and chamfering, respectively, the welding technique we propose does not require additional metal and groove preparation. The effects of the welding conditions on the intermetallic layer were studied by both optical and electron microscopes. One of the findings was that the solidified interface formed either from the Ti heat-affected zone and Al liquid or a Ti liquid and Al liquid interaction. Tomashchuk et al. (2015) presented the same result. The Vickers micro-hardness, tensile test and fracture surface analysis were analyzed to evaluate the mechanical behavior of the welds.

2. Experimental materials devices and procedure

2.1. Materials properties

The T40 and 5754 Al alloy plates were 1.5 mm thick. Tables 1–3 show the chemical composition, mechanical properties and thermo-physical properties of the two alloys.

Plate edges were saw-cut at low speed (1–3 mm/s) and polished with a 200 grit sandpaper in order to minimize the thermal contact resistance. This ensured that the contact conditions were both reproducible and uniform. Two parameters were determined to define the roughness characteristics with accuracy:

- the average roughness R_a, which is calculated as the mean of the absolute values of the deviation of the peaks from the midline;
- the maximum peak height R_y, which is determined as the maximum absolute value of the peaks.

Fig. 1(a) and (b) shows the roughness profile along the welding direction detected on the Ti and Al welding edges, respectively. As shown, Al sheet presented higher R_a and R_y than Ti.

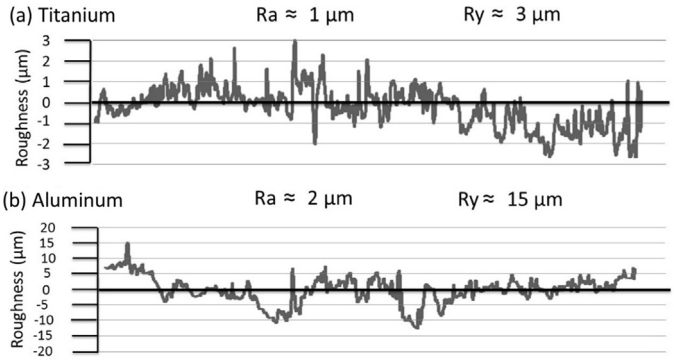

Fig. 1. Average roughness (R_a) and maximum peak height R_y profiles at the weld interface.

2.2. Laser equipment and welding set-up

A Yb–YAG laser (1.03 µm wavelength), was used in continuous wave regime. The maximum power was 3 kW. The laser beam was delivered to the workstation via a 200 µm diameter optical fiber and focused through an optical head equipped with collimating and focusing lenses with a 200 mm focal length. A slight defocusing (−2 mm) was used, resulting in an approximately 300 µm diameter (1/e2 width) near-Gaussian distribution on the top surface.

Fig. 2 shows a drawing of the welding layout. Top and bottom Argon gas protection was employed. The 20 l/min debit shielding gas sheltered the weld against air oxidation and contamination. Two adhesive tapes improved the protection. The laser beam was focused onto the Ti alloy plate. The offset between the center of the laser spot and the weld centerline varied initially between 0.5 and 1.4 mm. However, since preliminary tests revealed a lack of fusion between the welding edges, the offset upper-limit was set at 0.75 mm.

2.3. Process parameters

The experiment comprised a preliminary trial and two successive experimental plans (Tables 4 and 5) whose process parameters were determined according to the preliminary trial results. After the preliminary trial, the offset was limited to 0.5–0.75 mm because of lack of fusion between the welding edges. During the first experimental plan (Table 4), the laser offset was kept constant at 0.75 mm in order to assess the effect of the linear energy on the weld

Table 4
Process parameters for the first experimental plan (offset 0.75 mm).

Sample	Laser power (kW)	Welding speed (m/min)	Linear energy (J/mm)
1	1.50	1.60	56.24
2	2.00	1.80	66.67
3	1.75	2.00	52.50
4	1.75	1.80	58.33
5	1.50	2.00	45.00
6	1.50	1.80	50.00
7	2.00	2.00	60.00
8	2.00	1.60	75.00
9	1.75	1.60	65.62

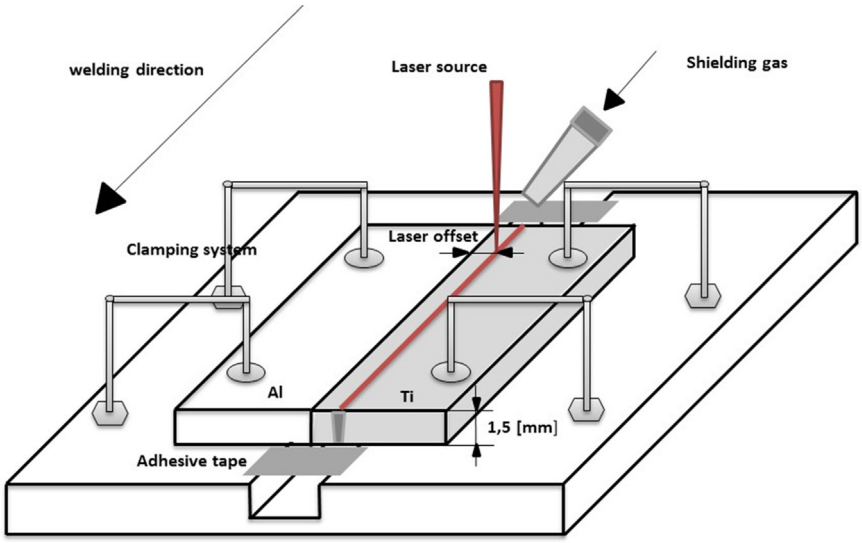

Fig. 2. Drawing of the welding device.

characteristics. The ratio of the laser power (P) to the welding speed (v) is the linear energy (LE).

Subsequently, the statistical significance of the linear energy and the laser offset and their interaction was tested by a two factors experimental design (DOE), whose parameters are reported in Table 5.

2.4. Sample preparation

Each weld was cross-sectioned perpendicularly to the welding direction, then polished and chemically etched in order to analyze the microstructure. Keller's reagent solution (1% HF, 1.5% HCl, 2.5% HNO_3 and 95% H_2O) was used for etching. Pictures of the microstructures were taken by optical (OM) and scanning electron microscope (SEM), which was equipped with an energy-dispersive X-ray spectrometer (EDS) to analyze the chemical composition.

Vickers micro-hardness was measured with a 400 g load. The hardness was taken at the mid thickness of the joint. The distance between two points was 0.25 mm. The dwell time was 10 s.

The tensile test was conducted using the INSTRON 5881 machine (Fig. 3) with a 10^{-4} s^{-1} strain rate. Three samples for each joint were cut perpendicularly to the welding direction. The tensile specimen had a 20 mm width and 200 mm length (Fig. 4). The mechanical strength and ductility were evaluated, as well as their robustness according to the welding conditions.

3. Results and discussion

3.1. Weld appearance

Fig. 5(a) and (b) shows the crown and root, respectively. The crown and root dimensions were in the range of 1.50–2.00 mm.

Table 5
Process parameters for the second experimental plan (laser power 1.5 kW).

Sample	Linear energy (J/mm)	Laser offset (mm)	Welding Speed (m/min)
10	36	0.75	2.5
11	36	0.50	2.5
12	30	0.50	3
13	30	0.75	3

The seam was regular and the amount of spatter was very low in comparison with the case in which the laser beam was focused on the Al side (Song et al., 2013; Alfieri et al., 2013)). Either the condensation of nanometer-size particles, which are contained in the vapor metal cloud during the keyhole regime, and the oxidation, which is due to the insufficient shielding of the molten pool, can explain the dark color of the region close to the interface. Further investigation by X-ray photoelectron spectroscopy can settle the issue. Despite the great affinity of Ti to oxygen, nitrogen and hydrogen, the local Ar shielding gas was useful to prevent the pool contamination.

Fig. 3. Tensile test machine.

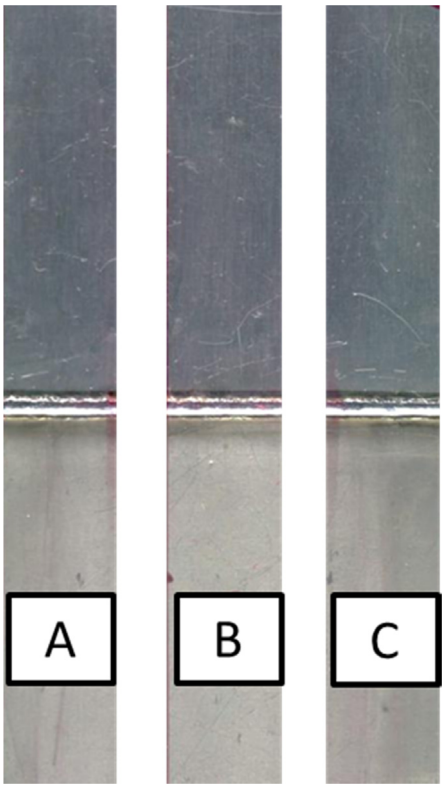

Fig. 4. tensile test specimens.

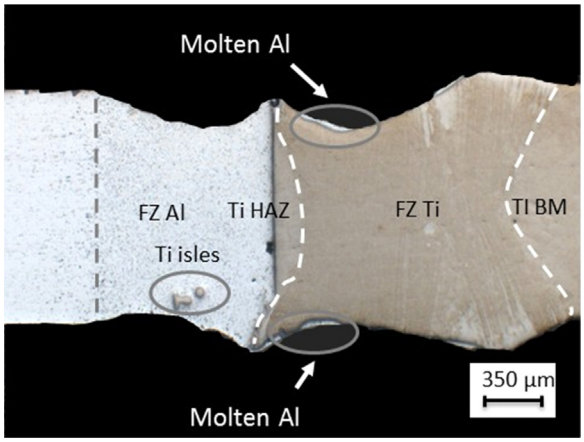

Fig. 6. Cross section of sample 5 (50.00 J/mm, 0.75 mm).

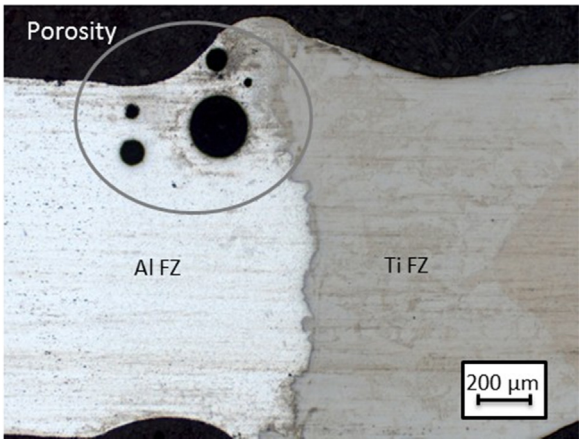

Fig. 7. Cross section of sample 11 (36 J/mm, 0.50 mm).

3.2. Microstructural characterization

3.2.1. Optical microscope analysis

Two different re-solidification conditions were observed in the Al after the keyhole formation in Ti.

In the first condition, the key-hole did not reach the Al. In this case, the heat was transmitted to the Al through the Ti HAZ. The re-solidification of the Al produced a straight, linear interface layer and continuity between the Ti HAZ and the Al FZ. However, the temperature was so high as to cause the diffusion of Ti in the Al matrix and the formation of intermetallic compounds. Fig. 6 shows the cross section of sample 5. The linear energy was 50.00 J/mm and the offset was 0.75 mm. The interface was Ti HAZ and the Al FZ and had a linear shape.

In the second condition, the heat input produced a keyhole in the Ti, whose fusion wall reached and melted the Al. This condition produced continuity between the Ti and the Al fusion zones (FZ) and a curvilinear interface layer. The curvilinear and irregular interface in Fig. 7 refers to sample 11. It was obtained with 36 J/mm linear energy and 0.50 mm offset. Moreover, macro-porosities formed in the Al sheet side, which drastically reduced the weld properties.

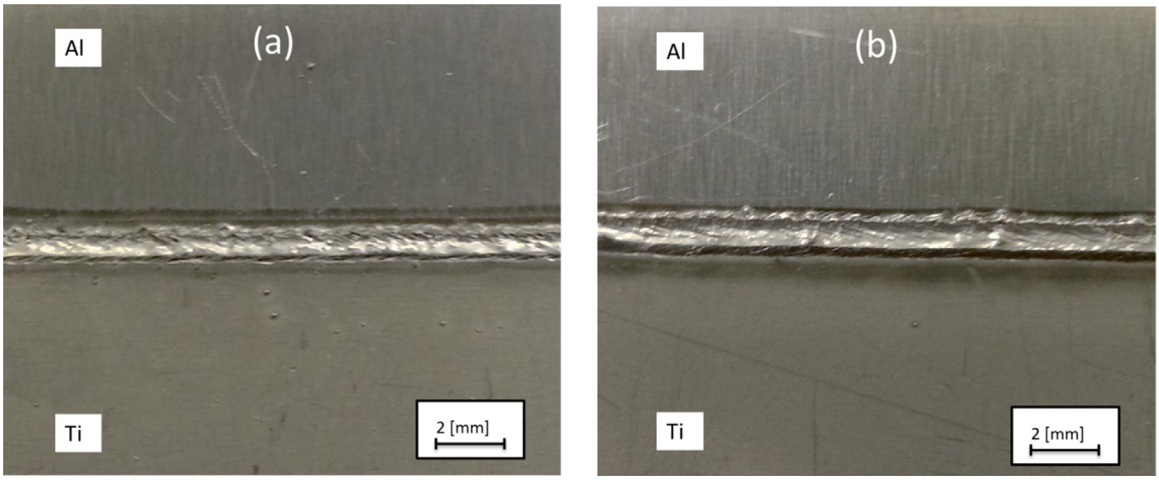

Fig. 5. Sample 6 (50 J/mm, 0.75 mm): (a) crown, (b) root.

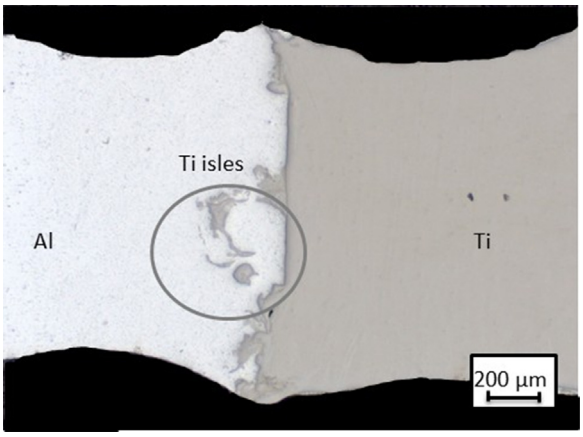

Fig. 8. Cross section of sample 3 (52.50 J/mm, 0.75 mm).

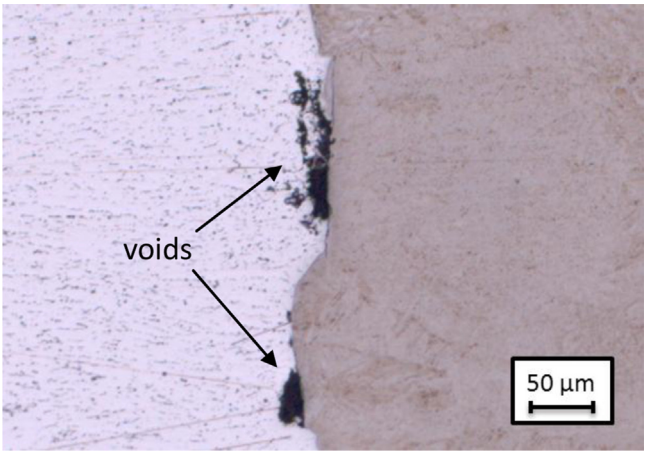

Fig. 9. Cross section of sample 8 (75 J/mm, 0.75 mm).

Ti isles formed in the Al FZ due to the direct liquid-liquid contact and the material convection flow, as shown in Fig. 8. After solidification, the agglomerates of Ti did not solubilize in the Al solid solution. Small Ti isles were also present on the Al side of the joint at a close distance from the interface (Fig. 6). This was probably due to the spattering of melted Ti that poured down on the Al side and remained caught up in the Al during its solidification.

A reduction in both the Ti and Al plate section occurred. For the Ti, the phenomenon was due to the keyhole formation. For the Al, it was due to the molten Al, which crept onto the Ti surface (Fig. 6).

Fig. 9 shows a micrograph of the cross section of weld 8, which was produced with a higher linear energy (75 J/mm). Some voids and microvoids formed at the intermetallic layer, from which cracks originated during the tensile test.

Pictures Fig. 10(a) and (b) shows two close-ups of the interface layer for different welding conditions. Fig. 10(a) refers to sample 1 that had a linear intermetallic layer. Some Ti lamellae protruded from the interface, starting towards the Al side. This phenomenon can be due to an enhanced local diffusion (short circuit-like) of the Ti into the molten Al. Fig. 10(b) shows a micrograph of sample 9, whose intermetallic layer was curvilinear. The Ti invaded the Al side in the proximity of the interface between the metals. Ti lamellae were also present at the Ti–Al uneven interface.

3.2.2. SEM and EDS analysis

Fig. 11(a) and (b) shows the microstructure observed at the SEM, with magnification factors of 2000× and 4000×, respectively.

Table 6
Chemical composition (atom percentage) at points indicated in Fig. 11a.

Point	Mg	Al	Ti	Other
A	1.2	56.6	41.6	0.6
B	1.6	68.0	29.9	0.5
C	2.9	63.0	33.6	0.5

Fig. 11(a) shows the location of the chemical analysis and Table 6 presents the correspondent EDS output.

The observation revealed that the chemical composition at point A, which contained both the Ti lamella and a small part of the surrounding Al alloy matrix, was 40% Ti and 60% Al. Points B and C were located approximately at the interface between the two alloys. Chemical analysis revealed 70% Al and 30% Ti. The higher percentage of Al in the examined points supports the formation of IMC, mostly made of $TiAl_3$.

Ti lamellae were produced under different welding conditions (Fig. 12(a) and (b), magnification 2000×). Higher linear energy tended to increase the dimension of Ti-based lamellae, which nucleated at the interface and grew towards the melted Al. The amount of Ti agglomerate in the Al side increased with the linear energy. The explanation is that the thermo-convective flow pushed semi-liquid Ti into the molten Al. The Ti does not mix with the Al because of the large surface tension and the viscosity difference between the two metals, i.e., the surface tension of molten Al is about 0.8 N/m (Bainbridge and John Andrew Taylor, 2013), while that of molten Ti is about 1.4 N/m (Man, 2000).

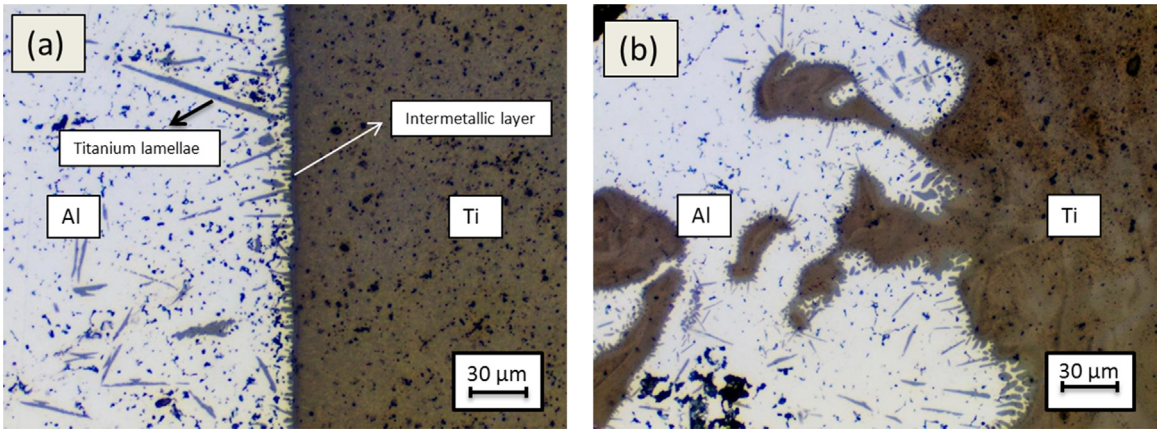

Fig. 10. Close-up of the intermetallic layer: (a) sample 1 (56.24 J/mm, 0.75 mm) with straight intermetallic interface, (b) sample 9 (65.62 J/mm, 0.75 mm) with irregular growth of the intermetallic layer.

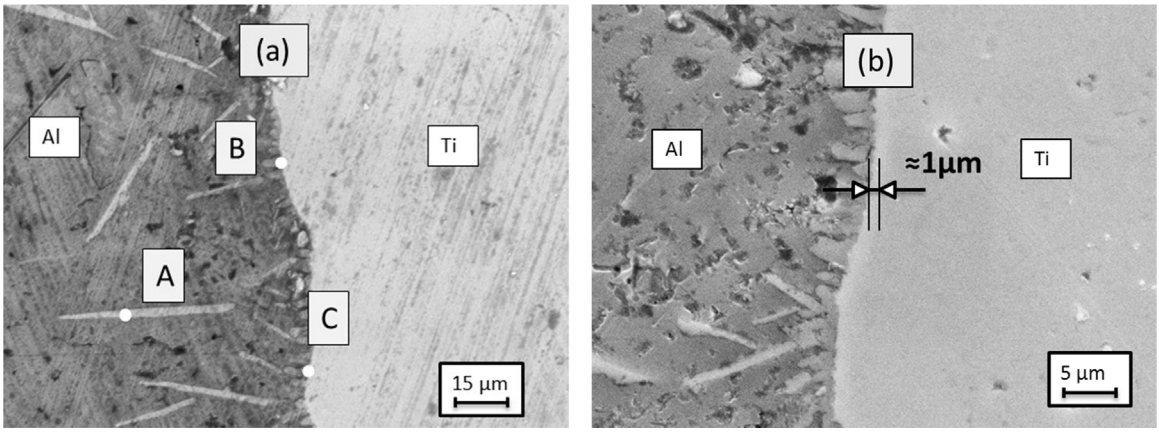

Fig. 11. SEM pictures of IM (a) sample 2 (66.67 J/mm, 0.75 mm), (b) sample 5 (45 J/mm, 0.75 mm).

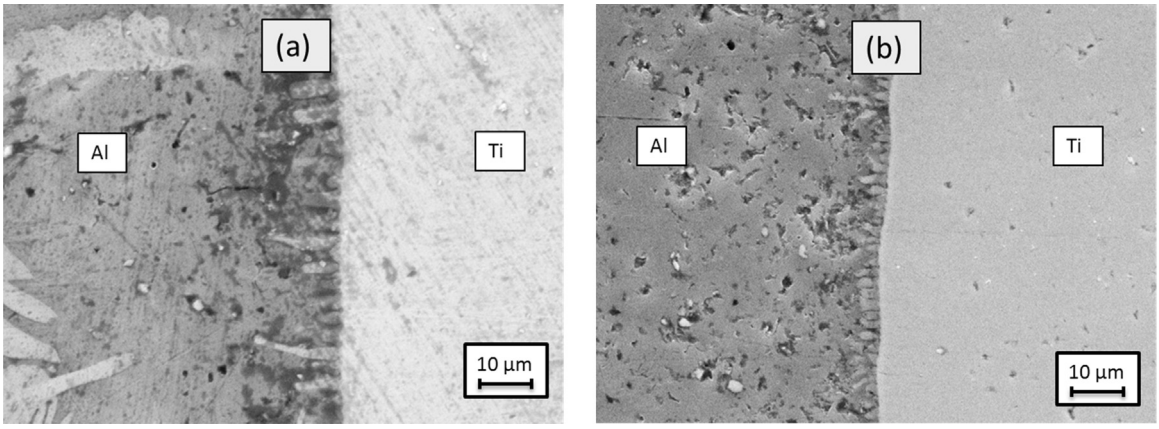

Fig. 12. SEM Micrograph: (a) sample 1 (56.24 J/mm, 0.75 mm), (b) sample 5 (45.00 J/mm, 0.75 mm).

3.3. *Mechanical properties and fracture analysis*

3.3.1. *Micro-hardness*

Fig. 13 represents the micro-hardness at the middle-thickness of the transverse cross section of sample 5. The Al fusion zone showed a micro-hardness that was slightly higher than the base material. The micro-hardness rose slightly because the grain was refined during the rapid solidification. Molten Ti produced local hardening. The hardness was greater in the FZ than in the Ti base material (250–300 $HV_{0.2}$ versus 180–200 $HV_{0.2}$). Because of the α_1 martensite phase, the Ti hardness increased up to 50% of that of the base metal (175 to 260 $HV_{0.2}$).

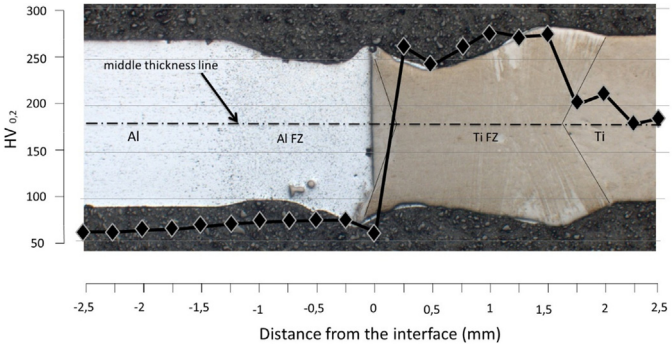

Fig. 13. Microhardness profile of sample 5 (45 J/mm, 0.75 mm).

Measurement of the micro-hardness within the intermetallic layer was impossible because the dimension of the impression was larger than the IM layer itself, which was ~1 µm (Fig. 14).

Fig. 14 shows the metals microstructure close to the intermetallic layer. Al FZ was made up of small-size grains with an inter-granular Mg precipitate. The microstructure of Ti was α_1 martensite, which produce during fast cooling. The intermetallic interface presented discontinuities.

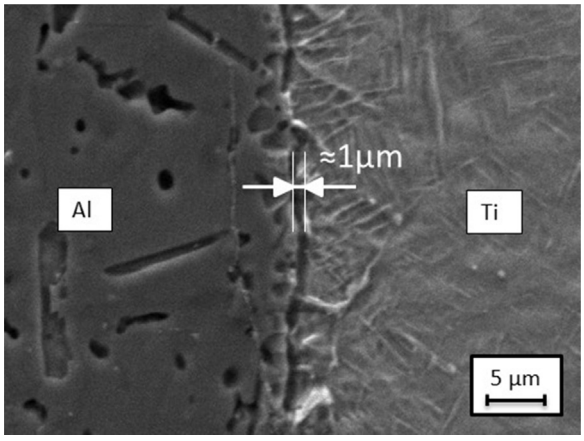

Fig. 14. Microstructure and interface of sample 5 (45 J/mm, 0.75 mm).

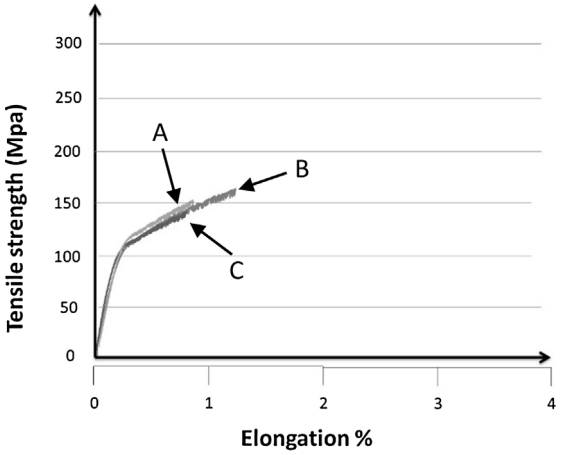

Fig. 15. Tensile test (samples A, B, C Fig. 4) for sample 4 (58.53 J/mm, 0.75 mm).

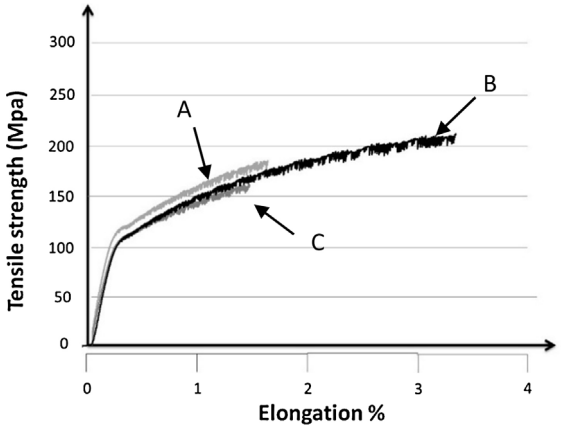

Fig. 16. Tensile test (samples A, B, C Fig. 4) for sample 6 (50.00 J/mm, 0.75 mm).

3.3.2. *Tensile test results*

Figs. 15 and 16 show the tensile strength curves for samples 4 and 6, which had J/mm linear energies of 58.00 and 50.00, respectively. Three specimens for each welding condition were analyzed and the means of the tensile strength and the elongation were measured (see Fig. 4 for the tensile sample appearance).

Figs. 17 and 18 present at-a-glance results of the tensile test for the experimental plans (Tables 4 and 5). The histograms also show the error bars, which display the maximum and minimum values for each measurement.

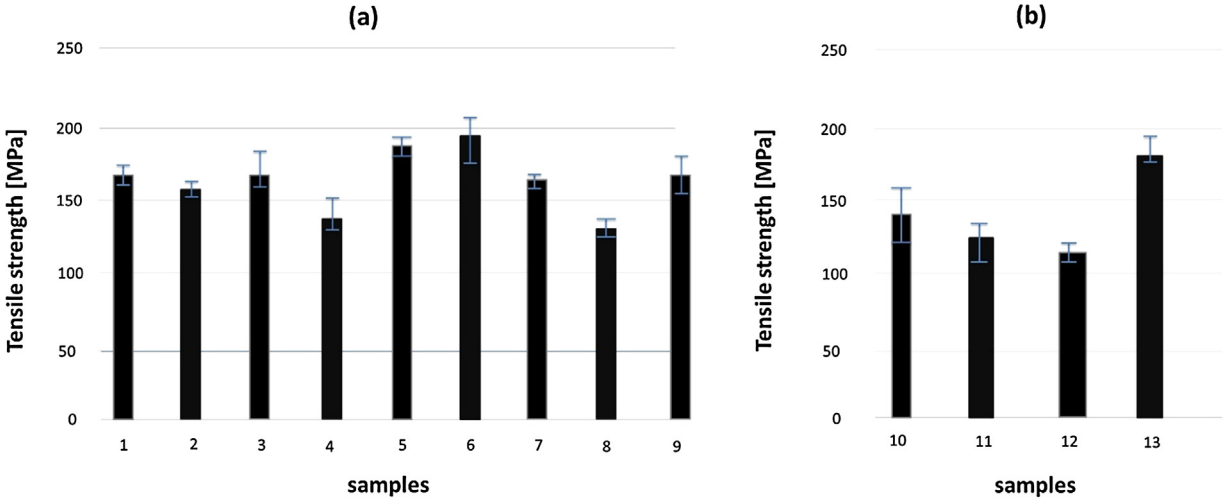

Fig. 17. Tensile strength of the samples of the (a) first and the (b) second experimental plan.

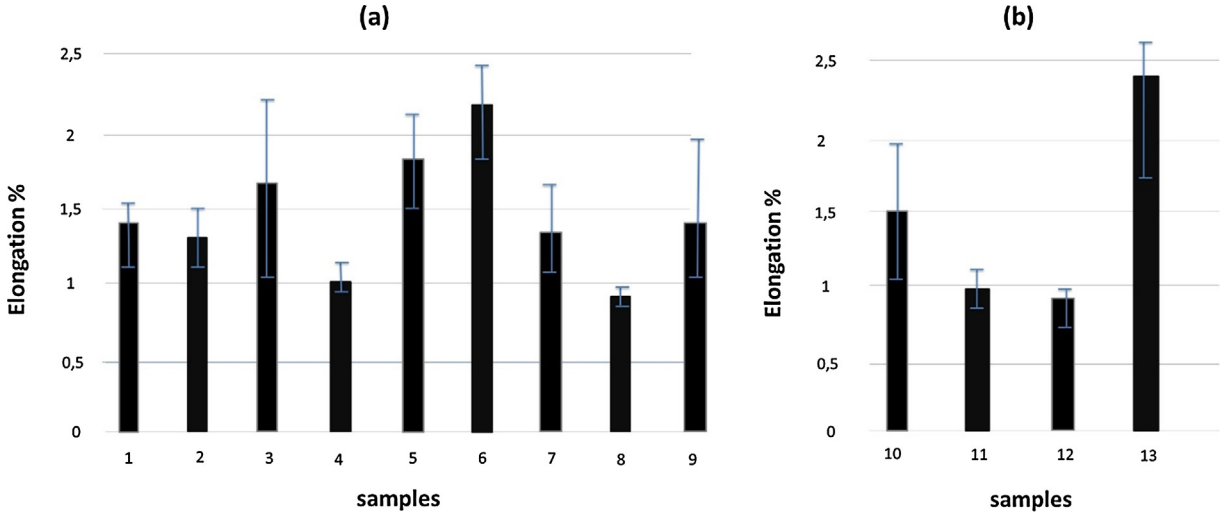

Fig. 18. Elongation % of the samples of the (a) first and the (b) second experimental plan.

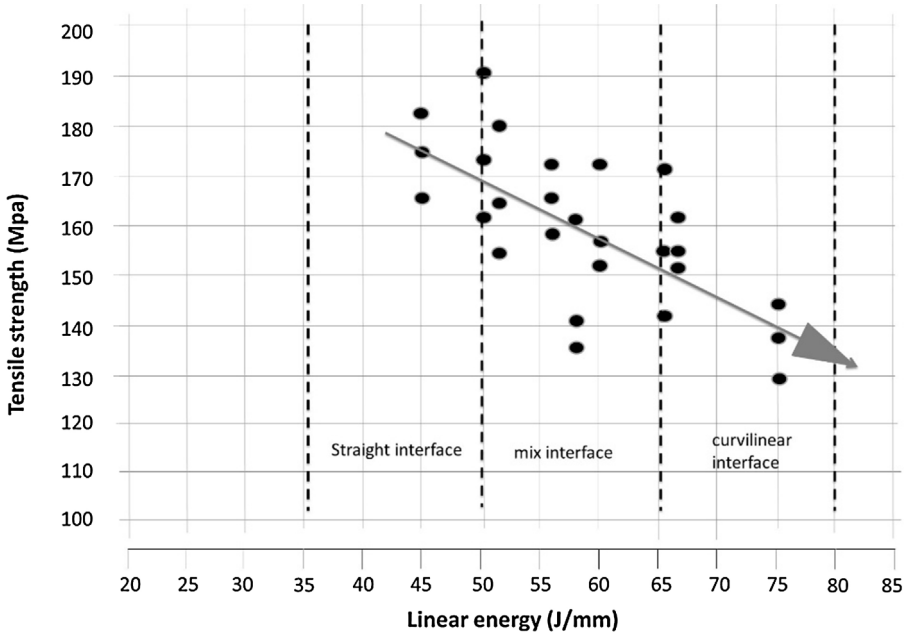

Fig. 19. Relation between the tensile strength and linear energy for 0.75 mm laser offset.

The process showed robustness in terms of ultimate tensile strength (UTS mean 160 MPa) and elongation (mean 1.5%). Simultaneous analysis of the microstructural characteristics of the welds and mechanical resistances values showed that joints with a curved interface layer tended to be less resistant. Phenomena involved near the interface, such as mixing of melted materials, alteration of the linearity of the interface and growth of Ti agglomerates and lamellae led to a reduction of the tensile strength.

Analysis of the tensile test revealed that the linear energy had a remarkable effect on the joint mechanical properties. A lower linear energy led to a significant increase of mechanical properties. Higher linear energy produced a liquid-liquid interaction that caused the growth of Ti agglomerates and lamellae that led to a reduction of the tensile strength and plasticity.

The reduction of mechanical properties was mainly due to the formation of IM compounds and mixing of materials during the process. Song et al. (2013) indicated a similar reduction of the tensile strength for Al–Ti joints, compared with as-received Al alloys.

The tensile strength achieved a peak of 191 MPa, which is almost 80% of the 5754 Al alloy UTS. That result was associated to a linear interface layer, low mix of materials and reduction of Ti lamellae in the Al FZ, which also slightly improved the ductility. In order to restore some ductility to the weld, a tailored heat treatment should act on the Ti lamellae dimension.

Figs. 19 and 20 show the variation of tensile strength and elongation values versus the linear energy for the first experimental plan (Table 4).

As shown in Figs. 19 and 20, low linear energy values increased the joint resistance and elongation. The explanation is that there

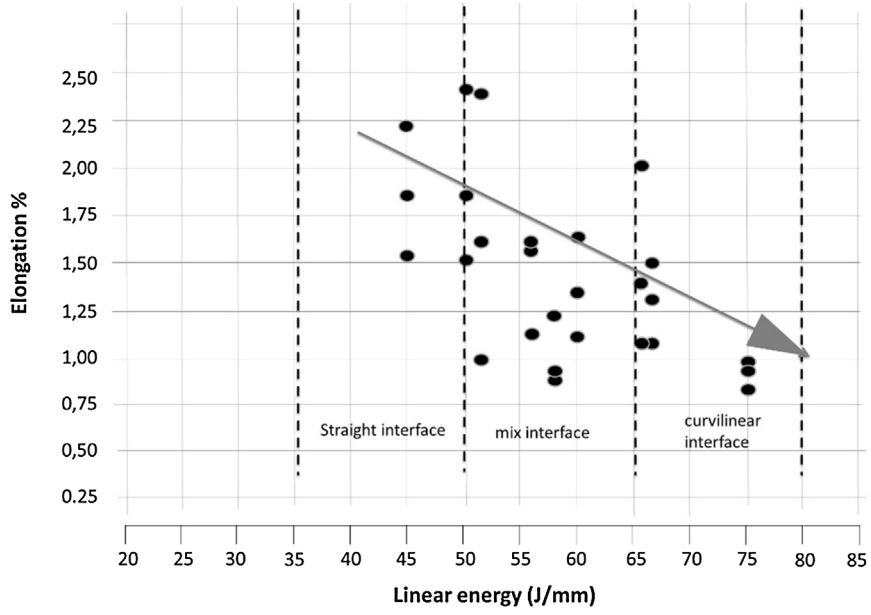

Fig. 20. Relation between the elongation and the linear energy for 0.75 mm laser offset.

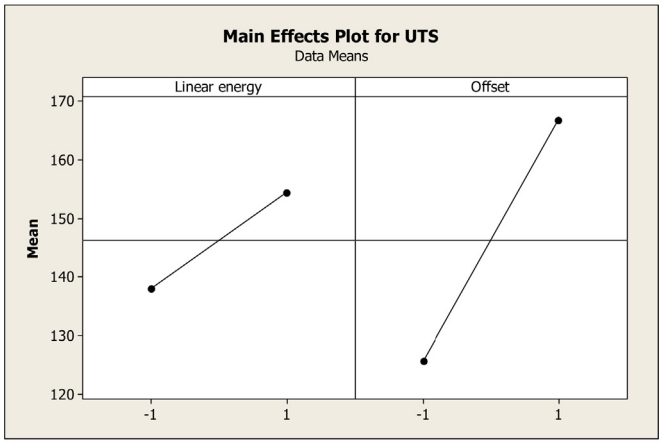

Fig. 21. Main effects plot for UTS.

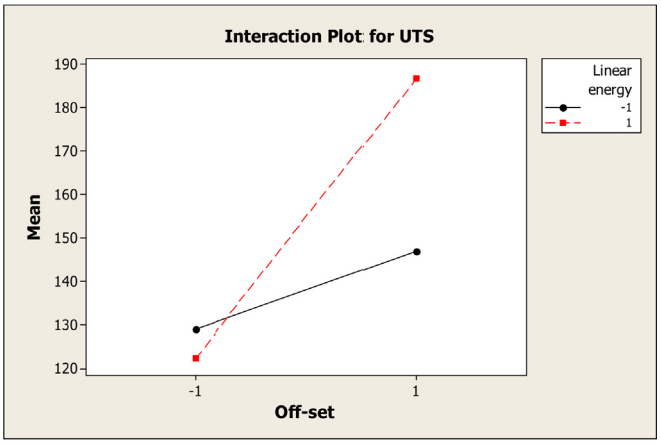

Fig. 22. Interaction plot for UTS.

was a decrease of the heat input, which led to a straight interface between the two metals. On the other hand, higher linear energy values resulted in a drastic reduction, which was due to a critical mixing and stirring of Ti and Al. The maximum resistance (191 MPa) and elongation (2.5%) were obtained with 50.00 J/mm linear energy.

Thomas and Bacos (2011) have suggested a microstructural refinement through a heat treatment to achieve higher mechanical properties for Ti–Al based alloys.

3.3.3. *Tensile test statistical analysis*

The second experimental plan (Table 5), was implemented in the form of the two-levels factorial design to study the effects of the linear energy, the laser offset and their interaction on the UTS. As Montgomery (2001) describes in his book, such an experimental plan must have two factors (linear energy and laser offset). Table 7 shows the levels and their design notation. In particular, symbol −1 marks a low level of the factor and symbol 1 a high level. Three repetitions of the tensile test were performed and the means of UTS were calculated for every welding condition. The results were statistically tested against the hypothesis that the welding factors had no significant relevance on the UTS.

Figs. 21 and 22 show the main effects and the interaction plots for UTS, respectively. The main effects plot shows the mean outcome, combining the effects of the other variables as if all variables were independent. The interaction plot illustrates the effects between dependent variables. The graphs proved the statistical significance of the main factors and their interaction, which means that a relationship between factors and UTS is real and not chance. The *p*-values, which is the probability that the factors had no effects on the UTS, are very low, see Table 8.The UTS means were higher for high levels of both the linear energy and the laser offset (Fig. 21).

Table 7
Two levels factorial design notation.

Sample	Linear energy (J/mm)	Laser offset (mm)
10	36 (1)	0.75 (1)
11	36 (1)	0.50 (−1)
12	30 (−1)	0.50 (−1)
13	30 (−1)	0.75 (1)

Table 8
p-Values for the statistical relevance of the effects.

Factor	*p*-Value (%)
Linear energy	0.024
Laser off-set	0.000
Interaction	0.004

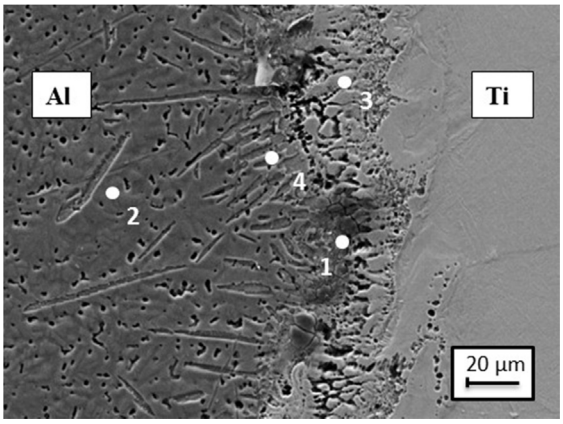

Fig. 23. Intermetallic layer.

When it comes to the interaction plot, the gain in terms of UTS was bigger for high level linear energy (1), than for low linear energy (−1) (Fig. 22).

3.3.4. *Fracture surfaces analysis*

The mode of fracture of Ti–Al welds depends on the morphology and phase composition of the contact interface (Tomashchuk et al., 2015). Several fractured surfaces were analyzed by SEM and EDS. The fracture occurred at the interface. Table 9 reports the chemical composition at some spots of the fractured surfaces. Observing the fracture surface, an opening fracture mode is inferable. Microvoids, which formed during the solidification, acted as stress raisers (Fig. 23).

Transgranular cleavage facets characterized the fracture surface (Fig. 24). Secondary microcracks were oriented perpendicularly to the major crack (Fig. 25). At point D, the Ti content was as high as 77.4% and Ti–Al compounds formed. High local tensile stress

Table 9
Chemical composition (atomic %, EDS) of some spots of fractured surface (Figs. 23 and 25).

Spot	Mg	Al	Ti
1	1.1	73.5	24
2	3.1	88	8.5
3	0.9	53.6	43.2
4	1.5	55.2	40.9
D	2.6	69.6	27.5
E	1.9	20.4	77.4

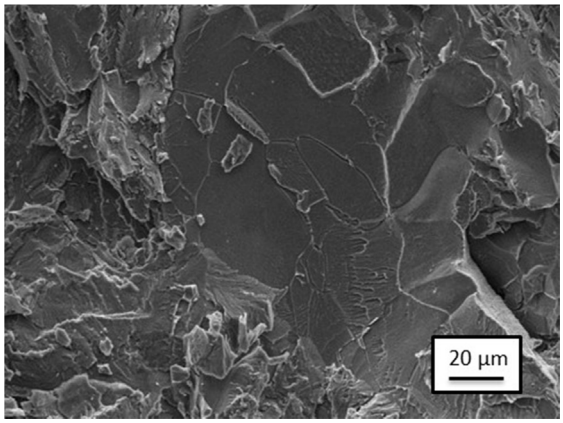

Fig. 24. Transgranular cleavage facet.

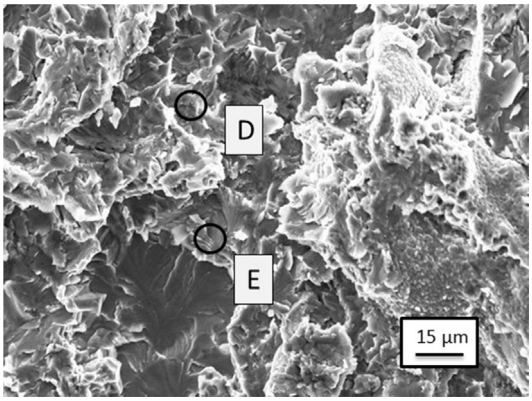

Fig. 25. Secondary microcrack (near point E).

was due to dislocation pile-up ahead of the Ti–Al compounds and contributed to the global final failure.

More microvoids, which formed at inclusions, intermetallic or second-phase particles and grain boundaries, coalesced. Growth and coalescence of those microvoids progressed as an intergranular crack (Fig. 26).

Based on these observations, it can be inferred that the brittle fracture initiation connected with the intergranular decohesion was the fracture micromechanism. Therefore, the fracture had both intergranular and trasgranular characteristics.The causes and characteristics governing the intergranular fracture initiation and occurrence of the fracture micromechanism in competition with the cleavage mechanism could be addressed in future work, following the example of Dlouhy et al. (2011), which studied the quantification of the transgranular/intergranular fracture by the relation of cleavage fracture and critical stresses.

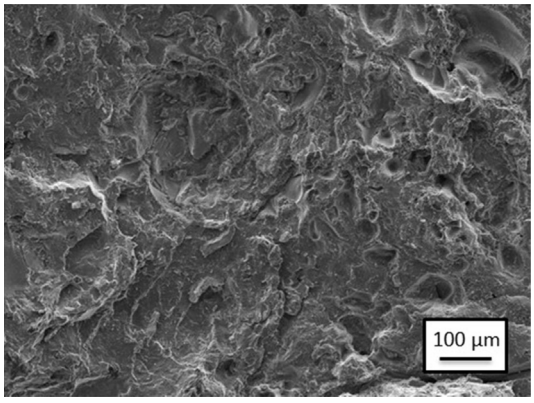

Fig. 26. Coalesced microvoids.

4. Conclusions

Al–Ti fiber laser offset welding (FLOW) consists in focusing a fiber laser beam onto the Ti side of the weld, close to its centerline. Neither filler metal nor groove preparation was necessary.

The investigation produced the following results.

- No occurrence of porosity and spatter in the Al alloy, as reported in several previous studies, was observed.
- The morphology analysis revealed linear and curvilinear IM layers, which depended on the energy input and laser offset. IM layer thickness was as small as1 µm, which has a negligible effect on the weld mechanical properties.
- The fracture occurred in the intermetallic layer with an opening fracture mode. Transgranular and intergranular fractures were observed.
- Mechanical properties decreased with the curvilinear intermetallic profile and increased with the linear profile. The linear energy, the laser offset and their interaction had statistical significance on UTS. In the present investigation, the maximum UTS was obtained with the 0.75 mm laser offset and 50 J/mm linear energy. It was as high as 191 MPa, which is in line with the best published results.

Therefore, the FLOW technique was demonstrated to be capable of producing a good quality and robust T40 and AA5754 weld, not requiring filler metal and chamfering.

Acknowledgements

This work was supported by the 2013 visiting professor program of the Ecole Normale Arts et Métiers of Paris, France.

References

Alfieri, V., Caiazzo, F., Sergi, V., 2013. Dissimilar joining of Ti alloy Ti–6Al–4V to Al alloy 2024 via laser welding. In: 32nd International Congress on Applications of Lasers and Electro-Optics, ICALEO 2013, 6–10 October, 2013, Miami, FL, United States.

Bondar, A.A., Witusiewicz, V.T., Hecht, U., Remez, M.V., Voblikov, V.M., Tsyganenko, N.I., Yevich, Ya. I., Podrezov, Yu. M., Velikanova, T.Ya., 2011. Structure and properties of Ti–Al alloys doped Wit-*/h niobium and tantalum. Powder Metall. Met. Ceram. 50, 7–8.

Bainbridge, I.F., John Andrew Taylor, J.A., 2013. The surface tension of pure Al and Al alloys. Metall. Mater. Trans. 44, 3901.

Chen, Yanbin, Chen, Shuhai, Li, Liqun, 2010. Influence of interfacial reaction layer morphologies on crack initiation and propagation in Ti/Al joint by laser welding–brazing. Mater. Des. 31, 227–233.

Chen, Shuhai, Li, Liqun, Chen, Yanbin, Dai, Jingmin, Huang, Jihua, 2011a. Improving interfacial reaction nonhomogeneity during laser welding–brazing Al to Ti. Mater. Des. 32, 4408–4416.

Chen, Yuhua, Liu, Changhua, Geping, Liu, 2011b. Study on the joining of Ti and Al dissimilar alloys by friction stir welding. Open Mater. Sci. J. 5, 256–261.

Dlouhy, I., Tarafder, M., Hadraba, H., 2011. Micromechanical aspects of transgranular and intergranular failure competition. Key Eng. Mater. 465, 399–402.

Dressler, Ulrike, Biallas, Gerhard, Mercado, Ulises Alfaro, 2009. Friction stir welding of Ti alloy TiAl6V4 to aluminium alloy AA2024-T3. Mater. Sci. Eng., A 526, 113–117.

Kreimeyer, Michael, Wagner Florian, X., Vollertsen, Frank, 2005. Laser processing of Al–Ti-tailored blanks. Opt. Lasers Eng. 43, 1021–1035.

Lee, Su-Jin, Nakamura, Hiroshi, Kawahito, Yousuke, Katayama, Seiji, 2013. Microstructural characteristics and mechanical properties of single mode fiber laser lap welded joint in Ti and Al dissimilar metal. Trans. JWRI 1, 17–21.

Luo, J.-G., Acoff, V.L., 2000. Interfacial reactions of Ti and Al during diffusion welding. Suppl. Weld. J. 79 (September), 239s–243s.

Man, K.F., 2000. Surface tension measurements of liquid metals by the quasi-containerless pendant drop method. Int. J. Thermophys. 21 (3), 793–804.

Ming, G., Cong, C., Yunze, G., Xiaoyan, Z., 2014. Microstructure and tensile behavior of laser arc hybrid welded dissimilar Al and Ti alloys. Materials 7, 1590–1602, http://dx.doi.org/10.3390/ma7031590

Möller, F., Grden, M., Thomy, C., Vollertsen, F., 2011. Combined laser beam welding and brazing process for aluminium Ti hybrid structures. Physics Procedia 12, 215–223.
Montgomery, D.C., 2001. Design and Analysis of Experiments, fifth ed. John Wiley & Sons Inc, New York, NY, USA.
Pastor, M., Zhao, H., Martukanitz, R.P., Debroy, T., 1999. Porosity, underfill and magnesium loss during continuous wave Nd:YAG laser welding of thin plates of Al alloys 5182 And 5754. Weld. Res. Suppl. 78, 207–216.
Peyre, P., Berthea, L., Dala, M., Pouzeta, S., Sallamand, P., Tomashchuk, I., 2014. Generation and characterization of T40/A5754 interfaces with lasers. J. Mater. Process. Technol. 214, 1946–1953.
Song Zhihua, Nakata Kazuhiro, Wub Aiping, Liao Jinsun, 2013. Interfacial microstructure and mechanical property of Ti6Al4V/A6061 dissimilar joint by direct laser brazing without filler metal and groove. Mater. Sci. Eng., A 560, 111–120.
Thomas, M., Bacos, M.-P., 2011. Processing and characterization of TiAl based alloys: towards an industrial scale. J. AerospaceLab 3, 1–11.
Tomashchuk, I., Sallamanda, P., Cicala, E., Peyre, P., Grevey, D., 2015. Direct keyhole laser welding of aluminum alloy AA5754 to titanium alloy Ti6Al4V. J. Mater. Process. Technol. 217, 96–104.
Vaidya, W.V., Horstmann, M., Ventzke, V., Petrovski, B., Koçak, M., Kocik, R., Tempus, G., 2010. Improving interfacial properties of a laser beam welded dissimilar joint of aluminium AA6056 and titanium Ti6Al4V for aeronautical applications. J. Mater. Sci. 45, 6242–6254.